$\delta^{18}O$ as a tracer of PO_4^{3-} losses from agricultural landscapes

Naomi S. Wells[1,2*], Daren C. Gooddy[3], Mustefa Yasin Reshid[1], Peter J. Williams[3], Andrew C. Smith[4], Bradley D. Eyre[1]

[1]Centre for Coastal Biogeochemistry, School of Environment, Science & Engineering, Southern Cross University, PO Box 157, East Lismore, 2480 NSW, Australia

[2]Department of Soil & Physical Sciences, Faculty of Agricultural & Life Sciences, Lincoln University, Lincoln 7647, New Zealand

[3]British Geological Survey, Wallingford, Oxfordshire, OX10 8BB, UK

[4]British Geological Survey, Keyworth, Nottinghamshire, NG12 5GG, UK

*Author for correspondence: naomi.wells@lincoln.ac.nz

Submitted to *Journal of Environmental Management*

Highlights

- Isotope fingerprints of soil and fertiliser PO_4^{3-} ($\delta^{18}O_P$) vary within catchments
- Source mixing and biological turnover affect $\delta^{18}O_P$ signatures exported downstream
- Tracing agricultural pollution with $\delta^{18}O_P$ requires accounting for soil zone dynamics

Abstract

Accurately tracing the sources and fate of excess PO_4^{3-} in waterways is necessary for sustainable catchment management. The natural abundance isotopic composition of O in PO_4^{3-} ($\delta^{18}O_P$) is a promising tracer of point source pollution, but its ability to track diffuse agricultural pollution is unclear. We tested the hypothesis that $\delta^{18}O_P$ could distinguish between agricultural PO_4^{3-} sources by measuring the integrated $\delta^{18}O_P$ composition and P speciation of contrasting inorganic fertilisers (compound v rock) and soil textures (sand, loam, clay). $\delta^{18}O_P$ composition differed between the three soil textures sampled across six working livestock farms: sandy soils had lower overall $\delta^{18}O_P$ values (21 ± 1 ‰) than the loams (23 ± 1 ‰), which corresponded with a smaller, but more readily leachable, PO_4^{3-} pool. Fertilisers had greater $\delta^{18}O_P$ variability (~8‰) driven by both fertiliser type and manufacturing year. Upscaling these values showed that 'agricultural soil leaching' $\delta^{18}O_P$ signatures could span from 18 – 25 ‰, and are influenced by both fertiliser type and the time between application and leaching. These findings emphasise the potential of $\delta^{18}O_P$ to untangle soil-fertiliser P dynamics under controlled conditions, but that its use to trace catchment-scale agricultural PO_4^{3-} losses is limited by uncertainties in soil biological P cycling and its associated isotopic fractionation.

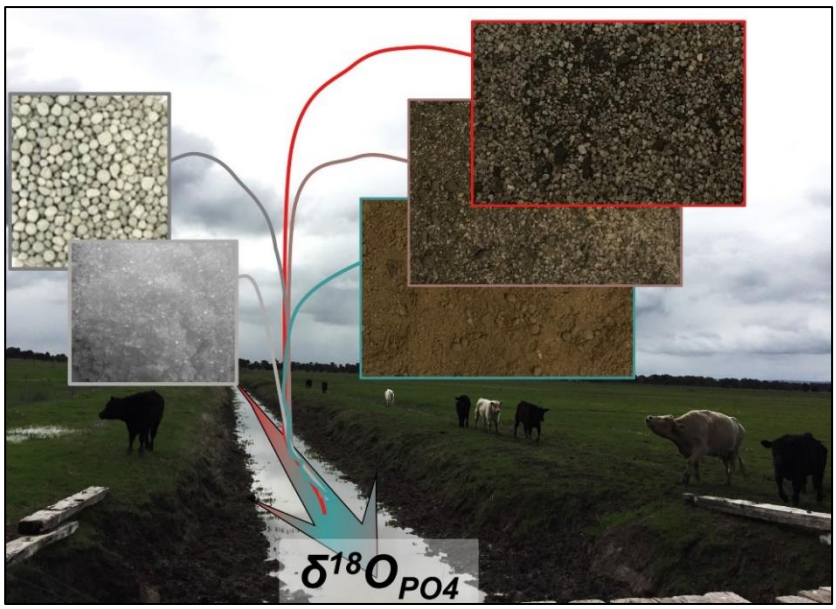

Keywords: Phosphate leaching, stable isotope tracers, eutrophication, diffuse agricultural pollution, Peel-Harvey catchment, $\delta^{18}O$-PO_4^{3-}

1. Introduction

Population growth and agricultural intensification has doubled phosphorus (P) inputs to global rivers (Beusen et al., 2016). While point source (e.g., wastewater treatment plants) P pollution can be effectively managed, diffuse P export from agriculture remains a pernicious water quality threat (Haygarth et al., 2005). This is in part due to the difficulty tracing P from its origin (e.g., fertiliser application) through the soil zone (where multiple biological and abiotic reactions can occur) to the receiving waters (Melland et al., 2018). New tools to identify excess P transported from soils to waterways via leaching and overland flow (henceforth 'export') are required to mitigate aquatic ecosystem degradation from eutrophication (e.g., hypoxia, fish kills).

Calls to use the isotopic composition of oxygen within PO_4^{3-} ($\delta^{18}O_P$) as a P tracer date back >10 years (Davies et al., 2014; Gruau et al., 2005; Young et al., 2009). This stems from evidence that PO_4^{3-} sources (wastewater, tap water, fertilisers) can have distinct $\delta^{18}O_P$ signatures (Gooddy et al., 2018; Gooddy et al., 2015; Granger et al., 2017b). Additionally, knowledge that intracellular reactions with phosphatase enzymes impart a predictable temperature-dependent equilibrium signature as oxygen is exchanged between PO_4^{3-} and the surrounding water (Chang and Blake, 2015; Gross and Angert, 2015; Jaisi et al., 2011), means $\delta^{18}O_P$ can also indicate ecosystems P cycling efficiency (Paytan et al., 2017; Pistocchi et al., 2017). Numerous studies propose using $\delta^{18}O_P$ source and transformation data to constrain catchment-scale P pollution dynamics (Gooddy et al., 2016; Granger et al., 2017b; Ishida et al., 2019; Tonderski et al., 2017). However, models are limited by uncertainty around the $\delta^{18}O_P$ 'signatures' generated by different catchment P sources.

Controls on agricultural soil $\delta^{18}O_P$ values are poorly understood. This is a critical knowledge gap as agricultural soils can dominate catchment P exports (Metson et al., 2017). Previous reviews show soil $\delta^{18}O_P$ ranges from 11 – 25 ‰ (Tian et al., 2020), and that agricultural soil $\delta^{18}O_P$ tends towards the higher end of the range predicted for biological equilibration with long-term soil water trends (Granger et al., 2017a; Ishida et al., 2019; Polain et al., 2018; Tamburini et al., 2010; Tian et al., 2020). Current models propose that systems reflect 'source' $\delta^{18}O_P$ values (e.g., fertilisers) when

PO_4^{3-} is in excess of biological demand, and shift towards equilibrium when PO_4^{3-} is limiting due to enhanced P recycling (Bauke, 2020). Yet $\delta^{18}O_P$ variability (~5‰ across a single paddock (Granger et al., 2017a)) suggests additional factors are at play. And if P limitation were the main determinant of $\delta^{18}O_P$ reaching equilibrium, soil $\delta^{18}O_P$ should correlate with PO_4^{3-} concentration, but this is not typically observed (Granger et al., 2017a; Tamburini et al., 2010; Tian et al., 2020). Fertilisers themselves cause further difficulty for defining the 'agricultural' $\delta^{18}O_P$ range: fertiliser $\delta^{18}O_P$ composition is variable (Gruau et al., 2005), but could account for up to 80 % of agricultural soil PO_4^{3-} exports (McLaren et al., 2016; Nash et al., 2019).

The aim of this study was to parameterise the potential of $\delta^{18}O_P$ to trace agricultural PO_4^{3-} export at the catchment scale. We hypothesised that fertiliser inputs and soil P fertility combine to create unique $\delta^{18}O_P$ signatures. We tested this by measuring the $\delta^{18}O_P$ composition of contrasting fertilisers and soils across an 1,800 km^2 catchment, then using mixing models to define the possible range of exported $\delta^{18}O_P$ created by variable management (fertiliser application), biology (PO_4^{3-} turnover), and hydrology (time before leaching, equilibrium $\delta^{18}O_P$ values).

2. Materials & Methods

2.1 Site description

Soil and fertiliser samples were collected from the 1,800 km^2 Peel-Harvey catchment in southwestern Australia (Supporting Information (SI) S1 for maps). The catchment is flat (slope: 0.0015), with negligible elevation or aspect differences. Soils are P deficient, but their P retention capacity varies with the underpinning geology: the alluvial soils have a clay texture and quickly chemically immobilise fertiliser P inputs, while P is easily exported from the sand textured soils formed on ancient dunes (Bolland and Allen, 1998; McArthur and Bettenay, 1974). The region has a Mediterranean climate: hot, dry summers (27°C, 190 mm rain) v cool, wet winters (18°C, 1,000 mm rain). Fertilising to compensate for P immobilisation (clays) or leaching (sands) has contributed

to the hyper-eutrophication of the Peel-Harvey Estuary (Valesini et al., 2019). Pasture soils still contain twice the optimal P range and leach 140 T P y^{-1} (Rivers et al., 2013).

2.2 Sample collection

Fertiliser isotopic variability ($\delta^{18}O_{P(fert)}$) was constrained by analysing synthetic P fertilisers from CSBP (Perth, Western Australia). These covered dominant fertiliser types: monoammonium phosphate (MAP), superphosphate (SP), and a proprietary compound fertiliser with 16% N, 9% P, 14% S (AG). All three are water soluble (Nash et al., 2019). AG and SP were obtained for five manufacturing years (2013-2017) and MAP from one year (2017). These fertilisers are the products available to farmers in the catchment, but the exact mix applied to the sampled plots is unknown.

Soil samples (0 – 10 cm) were collected from 21 paddocks with contrasting soil textures (clay, sand, loam) on six ~2 km^2 farms across the catchment (SI S1). Sampling was timed to winter (July 2017) when soil PO_4^{3-} export occurs (Summers et al., 1999). Management effects, including fertiliser contamination of the measured soil $\delta^{18}O_P$ composition ($\delta^{18}O_{P(soil)}$), were minimised by selecting farms with the same land use (beef grazing) and vegetation (ryegrass/clover pasture) participating in a multi-year P fertiliser minimisation trial. Triplicate samples (0-10 cm) spaced 10 m apart were collected over three transects from each paddock, and triplicates bulked to produce three samples per paddock, which were homogenised, sieved, and air dried. Around this period ten precipitation events were sampled for oxygen isotopes in water ($\delta^{18}O_{H2O}$).

2.3 Sample analyses

All 63 soils (21 paddocks x 3 replicates) were analysed for pH, organic matter, and P concentration. A subset of 25 soils, selected to cover the different farms and textures and using P concentration to identify representative samples, were analysed for $\delta^{18}O_{P(soil)}$.

Soil pH was measured in 2.5:1 deionised water:dry soil extracts. Soil organic matter was determined via ignition (550 C for 4 h), and total (P_{total}) and organic (P_{org}) P concentration measured

by extracting ignited v un-ignited soils with 1M H_2SO_4 (50:1) and measuring filtered extractant P concentration via ICP (Saunders and Williams, 1955). Because chemical bonding between PO_4^{3-} and the soil matrix means that the amount of PO_4^{3-} in P_{total} may not correspond to the amount of biologically available or leachable P, PO_4^{3-} concentrations were additionally measured in sequential extractions as per (Hedley et al., 1982) in order to parameterise potential export and turnover rates. This defines PO_4^{3-} by decreasing extractability as a proxy for availability (Gu and Margenot, 2020). Briefly, 2 g dry soil were extracted with 40 ml deionised water, 0.5M $NaHCO_3$ (pH 8.5), 0.1M NaOH, and 1M HCl. Tubes were agitated for 18 h (rotary shaker), centrifuged (15 minutes), filtered (Whatman 0.45 µm) into duplicate 12 ml vials, stored at 4°C, and PO_4^{3-} concentrations analysed via flow injection analysis after neutralising NaOH and $NaHCO_3$ extracts.

$\delta^{18}O_{P(soil)}$ was measured on the total PO_4^{3-} extractable with 1M HCl (P_{TIP}). This enabled us to directly compare values across strongly contrasting soil textures, as preliminary tests showed clays had insufficient H_2O extractable PO_4^{3-} for $\delta^{18}O_P$ analyses, while sands had insufficient PO_4^{3-} in the more tightly bound fractions. Using P_{TIP} is also advantageous because, by capturing the majority of soil PO_4^{3-}, it integrates the daily/seasonal P fluctuations observed in the more easily extracted fractions (Angert et al., 2011). So while sequential chemical extractions are useful indicators of the amount of soil PO_4^{3-} likely to be exported (Rupp et al., 2018) the P_{TIP} $\delta^{18}O_{P(soil)}$ provides a more robust and scalable soil 'fingerprint': extracted PO_4^{3-} 'fractions' not actually exist in soils as discrete pools (Gu and Margenot, 2020) and do not reflect the potential biological recycling over export-relevant timeframes (Helfenstein et al., 2020; Wang et al., 2021).

The $\delta^{18}O_P$ compositions of soils (n = 25) and fertilisers (n = 11) were measured following Tamburini et al. (2010) Extractions were carried out at BGS (Wallingford) and isotope analyses at BGS (Keyworth). Briefly, 25 g dry soil (or 2 g fertiliser) were extracted overnight with 100 ml 1M HCl, centrifuged, and filtered. Dissolved organic matter was removed with DAX resin (20 ml), then ammonium phospho-molybdate precipitated with 4.2M ammonium nitrate and ammonium molybdate (dissolved in ammonium citrate) and re-precipitated as magnesium ammonium

158 phosphate. After removing cations (AG50 X8 resin), silver phosphate (Ag_3PO_4) was precipitated
159 using 5 ml of silver ammine solution. Triplicate subsamples (300 µg) of the produced Ag_3PO_4 were
160 weighed into silver capsules and the $\delta^{18}O_P$ composition determined via thermal conversion
161 elemental analyser (TC-EA, ThermoFinnigan, Germany) at 1400°C with graphite and glassy carbon
162 chips, coupled to a Delta+XL mass spectrometer (ThermoFinnigan, Germany). Triplicates'
163 precision was ≤0.3‰. Sample CO yield relative to Ag_3PO_4 standards was checked to ensure
164 deviations <10%. $\delta^{18}O_P$ values were calculated with an internal Ag_3PO_4 standard, ALFA-1 ($\delta^{18}O$:
165 14.2‰). There are no international reference materials, so ALFA-1 was calibrated to the Ag_3PO_4
166 standard 'B2207' (Elemental Microanalysis Ltd.) from an inter-laboratory comparison. Oxygen
167 isotope ($^{18/16}O$) values are reported in δ ‰ v VSMOW.
168
169 2.4 Calculations
170 Soil organic carbon (C_{org}) was estimated as 0.516×loss-on-ignition (Jensen et al., 2018).
171 Mineralisation of P_{org} to PO_4^{3-}, which can affect $\delta^{18}O_{P(soil)}$ values (Gross and Angert, 2015), was
172 parameterised as $P_{min(14)}$ (net mineralisation over 14 days) (Achat et al., 2010) based on measured
173 soil organic v inorganic P composition (see SI S2). Data analyses were performed using R.v4.0 /
174 RStudio.v1.3.959. Differences between farms and soil textures were determined via one-way
175 ANOVA with an estimated marginal means post-hoc (Bonferroni adjusted), and correlations
176 between soil parameters via Pearsons test (Kassambara, 2020). Figures were produced using
177 ggplot2, patchwork, and munsell (Pedersen, 2019; Wickham, 2018; Wickham, 2016). Significance
178 is defined as $p<0.05$ and values are reported as mean ± standard deviation.
179
180 2.4.1 Equilibrium $\delta^{18}O_P$
181 $\delta^{18}O_P$ values produced due to equilibrium fractionation during extracellular P cycling
182 ($\delta^{18}O_{P(eq)}$) were calculated using Eq. 1, as per (Chang and Blake, 2015; Hacker et al., 2019):
183 (Eq. 1) $$\delta^{18}O_{P(eq)} = (\delta^{18}O_{H2O} + 1000)e^{\left(\frac{14.43*1000}{T} - 26.54\right)/1000} - 1000$$

where $\delta^{18}O_{P(eq)}$ is defined by temperature (T, in kelvin) and $\delta^{18}O_{H2O}$. Eq. 1 was solved two ways. First, because the P_{TIP} used for $\delta^{18}O_{P(soil)}$ likely integrates long-term site conditions (Helfenstein et al., 2018), $\delta^{18}O_{P(eq)}$ was calculated using long-term records of soil temperature at 10 cm (mean: 21°C, high: 26°C, low: 18°C) and $\delta^{18}O_{H2O}$ (mean: -3.96 ‰, low: -2.74 ‰, high: -5.18 ‰, based on monthly precipitation $\delta^{18}O_{H2O}$ and amounts 1986-2012 for Perth, WA (Hollins et al., 2018; IAEA/WMO, 2020)). Second, because loosely bound PO_4^{3-} in the sandy soils could be turning over daily→seasonal intervals, $\delta^{18}O_{P(eq)}$ was also calculated using modelled daily winter soil temperatures (mean: 13ºC, high: 21ºC, low: 8.2ºC) (Kearney, 2019) and precipitation $\delta^{18}O_{H2O}$ values measured during sampling ($\delta^{18}O_{H2O}$: -3.07 ± 2 ‰, n = 10). Precipitation $\delta^{18}O_{H2O}$ was converted to soil water $\delta^{18}O_{H2O}$ based on evidence that soil $\delta^{18}O_{H2O}$ is a mass balance of seasonal precipitation (Benettin et al., 2018), ± +3‰ evaporative enrichment (Sprenger et al., 2017; Wan and Liu, 2016). See SI S3 for input data.

2.4.2 Export models

The possible $\delta^{18}O_P$ range exported from farms to waterways ($\delta^{18}O_{P(export)}$) was determined using a two end-member mixing model that considered a range of fertilisers (type and application rate), times between fertiliser application and PO_4^{3-} export, and soil biological P turnover (Fig. 1).

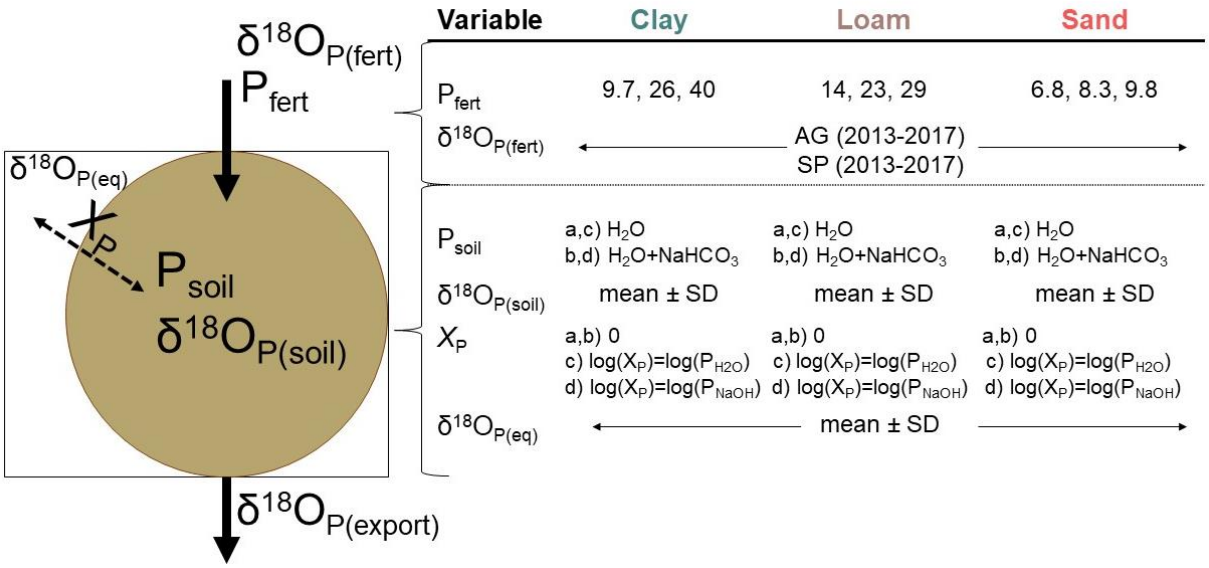

Fig. 1 Two-pool isotope mixing models (Eq. 2, Eq. 3) constrained the possible $\delta^{18}O_P$ range of PO_4^{3-} exported (leaching, run-off) from fertilised soils ($\delta^{18}O_{P(export)}$). The model was solved using recommended low, moderate, and high fertiliser applications rate (P_{fert}, in µg P g^{-1} soil) for each soil texture (clay, loam, sand) and $\delta^{18}O_{P(fert)}$ values for two fertilisers (AG: N-P-K, SP: superphosphate) manufactured between 2013 and 2017. $\delta^{18}O_{P(fert)}$ for each year × fertiliser were 'mixed' with each soil texture using the measured $\delta^{18}O_{P(soil)}$ range for P_{TIP} and P_{soil} (µg P g^{-1} soil), defined by H_2O extractable PO_4^{3-} for fast export scenarios (a, c) and H_2O + $NaHCO_3$ extractable PO_4^{3-} for slow/seasonal export scenarios (b, c). $\delta^{18}O_{P(export)}$ for both fast and slow export was calculated with (c, d) and without (a, b) soil biological P turnover (X_P), which shifts $\delta^{18}O_{P(export)}$ towards $d^{18}O_{P(eq)}$ (Eq. 1). Fast export X_P (c) was approximated by $[P_{H2O} \cdot e\text{^}(\log(100+P_{H2O})/100 \cdot 1)]/P_{TIP}$ and slow export X_P (d) by $[P_{NaOH} \cdot e\text{^}(\log(100+P_{NaOH})/100 \cdot 1)]/P_{TIP}$. Arrows indicate the same values were applied across all soil textures, otherwise soil-specific values (mean±SD) were used. See SI S4 for model scripts.

The $\delta^{18}O_{P(export)}$ range was first defined assuming no biological turnover prior to export (Eq. 2):

$$\text{(Eq. 2)} \qquad \delta^{18}O_{P(export.1)} = f_{fert}\delta^{18}O_{P(fert)} + f_{soil}\delta^{18}O_{P(soil)}$$

$$1 = f_{fert} + f_{soil}$$

$$f_{fert} = P_{fert}/P_{soil}$$

where f_{fert} and f_{soil} are the contribution of PO_4^{3-} from fertiliser and soil, respectively, and $\delta^{18}O_{P(fert)}$ and $\delta^{18}O_{P(soil)}$ their isotopic composition; f_{fert} was estimated for each soil texture based on its leachable soil P content (P_{soil}) and the recommended fertiliser application amount (P_{fert}). Two P_{soil} scenarios were considered: scenario a (fast), where export occurs within ~1 day of application (P_{soil} = H_2O extractable PO_4^{3-}), and scenario b (slow), where export occurs gradually over a whole season (P_{soil} = H_2O + $NaHCO_3$ extractable PO_4^{3-} (Rupp et al., 2018)).

Next, scenarios a and b were rerun to consider biological P turnover pushing $\delta^{18}O_P$ values towards $\delta^{18}O_{P(eq)}$, as per (Helfenstein et al., 2018):

(Eq. 3) $$\delta^{18}O_{P(export.2)} = X_P \cdot \left(\delta^{18}O_{P(eq)} - \delta^{18}O_{P(export.1)}\right) + \delta^{18}O_{P(export.1)}$$

where an exchange factor (X_P) defines $\delta^{18}O_{P(export.1)}$ mixing with $\delta^{18}O_{P(eq)}$ (Gross and Angert, 2015). Eq. 3 constrains the effects of short-term (daily to monthly) biological P cycling, so $\delta^{18}O_{P(eq)}$ was defined based on diurnal variations in winter soil temperatures (Eq. 1). As X_P is challenging to measure directly, values were approximated for each soil texture based on soil P mean residence time, calculated as the log-log linear relationship between H_2O extractable PO_4^{3-} and PO_4^{3-} turnover in <1 hr, or, 2) NaOH extractable PO_4^{3-} and PO_4^{3-} turnover in >1 hr – 3 months (Helfenstein et al., 2020). For biologically active 'fast' export (scenario c), X_P was defined as PO_4^{3-} exchange in < 1 hr and applied to scenario a $\delta^{18}O_{P(export.1)}$ values. For biologically active 'slow' export (scenario d), X_P was defined as the proportion of PO_4^{3-} exchange in 1 hr – 3 months and applied to scenario b $\delta^{18}O_{P(export.1)}$ values.

$\delta^{18}O_{P(fert)}$ variability was parameterised two ways. First, models were run using the annual differences in $\delta^{18}O_{P(fert)}$ measured 2013-2017 for different fertiliser types (AG and SP, but not MAP because only one year was sampled). Second, P_{fert} was varied to reflect the low, high, and median fertiliser application rates recommended for each soil texture: 14, 58, 37 kg P ha^{-1} (clay), 18, 37, 28 kg P ha^{-1} (loam), and 9, 13, 11 kg P ha^{-1} (sand) (Summers and Weaver, 2011). Application rates (kg P ha^{-1}) were converted to concentrations (µg P g^{-1}) in the top 10 cm of soil (P_{fert}) using regional pasture soil bulk density (Viscarra Rossel et al., 2014): 1.44 ± 0.2 kg ha^{-1} (clay), 1.25 ± 0.2 kg ha^{-1} (loam), and 1.33 ± 0.1 kg ha^{-1} (sand). This model does not consider the complex soil chemical processes affecting long-term fertiliser mobility, meaning fertiliser contributions to 'slow' export scenarios (b, d) may be overestimated.

Variability in soil inputs was parameterised by solving each export scenario (a: fast, b: slow, c: fast + turnover, d: slow + turnover) using the mean, mean+SD, and mean-SD of $\delta^{18}O_{P(soil)}$ and P_{soil} for each soil texture, as well as for $\delta^{18}O_{P(eq)}$ (Henry and Wickham, 2020): f_{fert} was calculated for each P_{soil} and P_{fert} combination, the minimum, mean-SD, mean, mean+SD, and maximum f_{fert} for scenarios (a, b) × soil texture used to solve Eq. 2 for each fertiliser × manufacturing year, and then

$\delta^{18}O_{P(export.1)}$ values used to solve Eq. 3 for scenario (c, d) × soil texture for each fertiliser × manufacturing year (Fig. 1). Output $\delta^{18}O_{P(export)}$ ranges were upscaled to possible 'agricultural soil' signatures based on the measured PO_4^{3-} content and spatial coverage of soil textures for two sub-catchments with contrasting soil distributions, see SI Fig. S2 (McArthur and Bettenay, 1974; Weller, 2019). Upscaling calculations varied the contribution of AG v SP fertilisers and timing between fertilisation and export (a: fast v d: slow + turnover).

3. Results

3.1 Fertilisers

Fertiliser types had different $\delta^{18}O_{P(fert)}$ values ($p<0.05$, F = 52). Values ranged from 17 ± 1 ‰ (SP) to 22 ± 0.05 ‰ (MAP) (Table 2). The $\delta^{18}O_{P(fert)}$ composition of SP and AG varied between manufacturing years: SP from 16 ± 0.2 ‰ in 2015 to 19 ± 0.2 ‰ in 2013, and AG from 20 ± 0.4 ‰ in 2014 to 22 ± 0.01 ‰ in 2015.

3.2 Soils

Soil pH was higher in clays than in loams or sands ($p<0.05$, F = 5.2) (Table 1). C_{org} was higher in clays (66 ± 20 mg C g^{-1}) than loams (40 ± 10 mg C g^{-1}) and sands (38 ± 30 mg C g^{-1}) (F = 2.7, $p<0.05$) (Table 1), as was P_{total} (clay: 360 ± 20 µg g^{-1}, loam: 190 ± 90 µg g^{-1}, sand: 120 ± 100 µg g^{-1}) (F = 20, $p<0.05$). P_{org} did not differ between soil textures or farms (SI Table S1), so P_{org} accounted for a higher proportion of P_{total} in sands (57 ± 10 %) than loams (45 ± 10 %) and clays (41 ± 0.09 %) (F = 12, $p<0.01$). The C_{org}:P_{org} ratio was higher in sands (630 ± 500 g/g) than in clays (540 ± 300 g/g) or loams (530 ± 200 g/g) (F = 3.3, $p<0.01$; Table 1). $P_{min(14)}$ was highest in absolute (F = 10, $p<0.05$) terms in sands (SI Table S3), and decreased as a proportion of P_{TIP} from sands (14 ± 10 mg g^{-1}) to loams (4.4 ± 3 mg g^{-1}) to clays (0.74 ± 0.4 mg g^{-1}) (F = 23, $p<0.001$; Table 1).

P_{TIP} (based on H_2O+$NaHCO_3$+NaOH+HCl fractions) was higher in clays (150 ± 90 µg P g^{-1}) than loams (53 ± 50 µg P g^{-1}) or sands (55 ± 80 µg P g^{-1}) (F = 11, $p<0.05$; Fig. 2). Water extractable

280 PO_4^{3-} differed between soil textures (F = 9.6, p<0.05), with concentrations in sands (11 ±10 µg P g^{-1})
281 higher than in loams (4.2 ± 3 µg P g^{-1}) and clays (1.7 ± 2 µg P g^{-1}) (Fig. 2). $NaHCO_3$ extractable
282 PO_4^{3-} did not differ between soil textures, but differed between farms (F = 3.0, p = 0.019): heavy
283 clay soils in F6 had the lowest concentrations (7.6 ± 4 µg P g^{-1}) and the predominantly sand soils in
284 F1 had the highest (27 ± 20 µg P g^{-1}) (see SI S2 for farm-level data). Clays had higher NaOH
285 extractable PO_4^{3-} (89 ± 50 µg P g^{-1}) than loams (29 ± 30 µg P g^{-1}) or sands (9.5 ± 10 µg P g^{-1}) (F =
286 26, p<0.001). Likewise, HCl extractable PO_4^{3-} was the highest in clays (39 ± 20 µg P g^{-1}) and the
287 lowest in loams (6.0 ± 8 µg P g^{-1}) (F = 3.9, p<0.05). 30% of P_{TIP} was H_2O extractable in sands,
288 versus 10% in loams and 1% in clays (F = 28, p<0.001; Fig. 2). The proportion of P_{TIP} in the
289 H_2O+$NaHCO_3$ fraction also decreased from sands (54 ± 20 %) to loams (41 ± 20 %) to clays (13 ±
290 5 %) (F = 40, p<0.001; Fig. 2). X_P (Eq. 3) estimated for <1 hr was 30% (sand), 10% (loam), and 1%
291 (clay), while X_P estimated for turnover >1 hr – 3 months was 20% (sand), 60% (loam), and 90%
292 (clay), see SI Table S7.

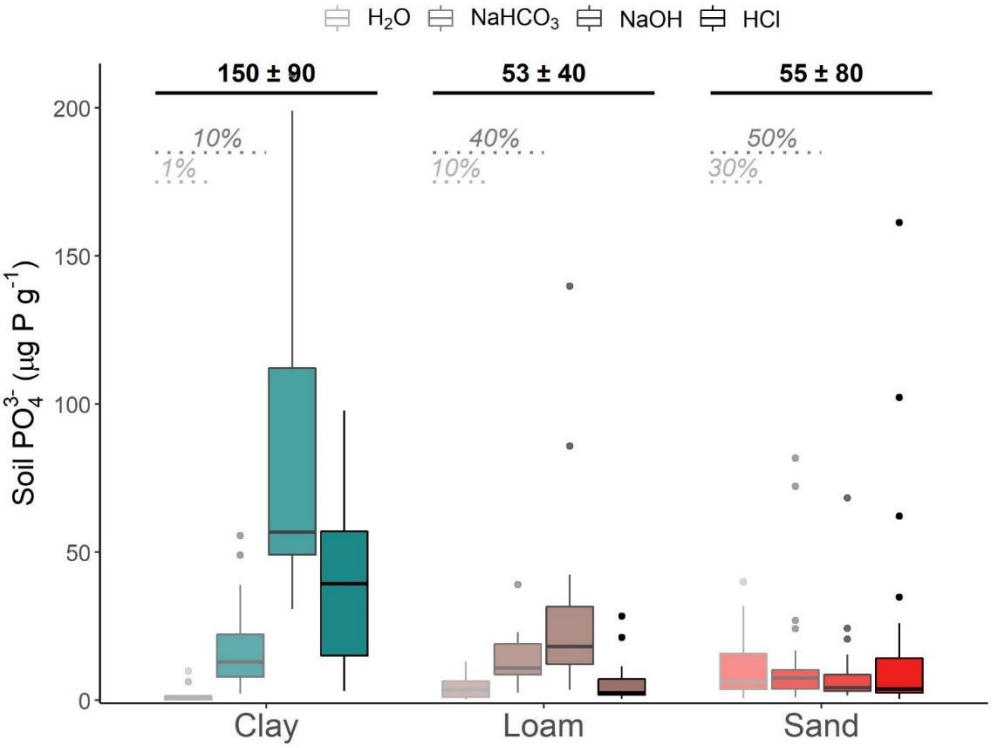

293

294 **Fig. 2** Phosphate in surface soils (0 – 10 cm) of 21 pastures with different soil textures in the Peel-Harvey catchment
295 (Western Australia) based on sequential extraction with H_2O (left, light outline), $NaHCO_3$, NaOH, and HCl (right, dark
296 outline). P_{TIP} concentrations (sum of four fractions) for each soil textures is indicated at the top, and the percentage
297 contribution of H_2O (easily leachable) and H_2O+$NaHCO_3$ (seasonally leachable) fractions indicated with dashed lines.
298 Boxes represent median ± 1 SD.

$\delta^{18}O_{P(soil)}$ values ranged from 25.3‰ (F4 loam) to 17.9‰ (F2 sand). Values negatively correlated with $P_{min(14)}$ ($p = 0.03$, $r = -0.45$) and positively correlated with C_{org} ($p = 0.03$, $r = 0.5$). Soil P concentrations did not correlate with $\delta^{18}O_{P(soil)}$. $\delta^{18}O_{P(soil)}$ values differed between soil textures but not farms, and were higher in loams (23.2 ± 1 ‰) than clays (22.3 ± 0.9 ‰) or sands (21.4 ± 2 ‰) ($p<0.05$; F = 3.8; Fig. 3). $\delta^{18}O_{P(eq)}$ values calculated using long-term temperature and $\delta^{18}O_{H2O}$ records ranged from 16.9 to 23.8 ‰ (20.4 ± 1.97 ‰), versus from 19.3 – 24.1 ‰ based on winter soil temperatures and $\delta^{18}O_{H2O}$ (Fig. 3). This places loam $\delta^{18}O_{P(soil)}$ values at or above the maximum $\delta^{18}O_{P(eq)}$ range, versus sand $\delta^{18}O_{P(soil)}$ values around mean $\delta^{18}O_{P(eq)}$.

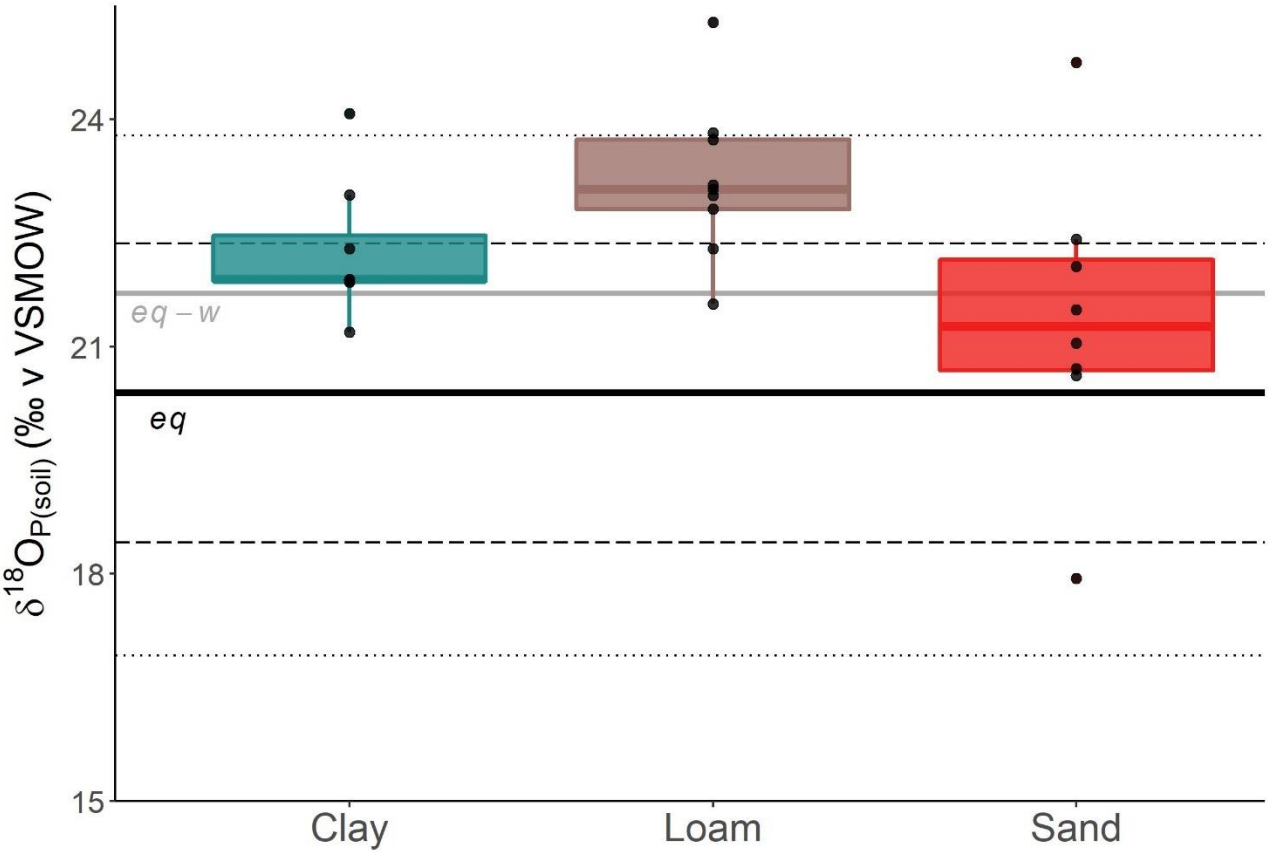

Fig. 3 The $\delta^{18}O_P$ of P_{TIP} in pasture soils (0-10 cm) classed as either clay, loam, or sand from six farms across the Peel-Harvey catchment (Western Australia). Boxes represent median ± 1 SD for each soil textures. Black lines represent the mean (solid line), ±1 SD (dashed lines), and minimum/maximum (dotted lines) of the long-term local $\delta^{18}O_{P(eq)}$ range (Eq. 2); the grey line indicates the mean $\delta^{18}O_{P(eq)}$ calculated for conditions during the winter sampling (*eq-w*).

315 3.3 Export model

316 For scenario (a), f_{fert} (Eq. 2) decreased from 0.93 ± 0.1 (clays) via 0.84 ± 0.1 (loams) to 0.54
317 ± 0.2 (sands) (Fig. 4a). For scenario (b), f_{fert} was 0.57 ± 0.1 for clays, 0.57 ± 0.1 for loams, and 0.37
318 ± 0.2 for sands (Fig. 4b). In scenario (a) $\delta^{18}O_{P(export)}$ values track $\delta^{18}O_{P(fert)}$, with clear differences
319 between AG v SP applied to all soil textures (Fig. 4c). Rapid P turnover (scenario c) shifted sand,
320 but not clays or loams, $\delta^{18}O_{P(export)}$ away from low-end $\delta^{18}O_{P(fert)}$ values (Fig. 4e). Yearly $\delta^{18}O_{P(fert)}$
321 differences in SP (2013 v 2014-2017) and AG (2014 v 2015) fertilisers affected modelled
322 $\delta^{18}O_{P(export)}$ from clays and loams, but not sands, under 'fast' scenarios (a, c) (Fig. 4c,e). For 'slow'
323 scenarios (b, d), differences in SP v AG $\delta^{18}O_{P(export)}$ values were only expressed when X_P = 0% (Fig.
324 4d), and $\delta^{18}O_{P(export)}$ from all soil textures and fertilisers normalised to $\delta^{18}O_{P(eq)}$ with ~monthly P
325 turnover (Fig. 4f). Upscaling to sub-catchments, the possible $\delta^{18}O_{P(export)}$ range is narrowest (~2‰)
326 if export is slow and fertilisation type uniform (Table 3). In both sub-catchments fertiliser mixing
327 was more important than the export speed in defining the $\delta^{18}O_{P(export)}$ values, and mixed fertilisers +
328 slow export produced the widest possible $\delta^{18}O_{P(export)}$ range.

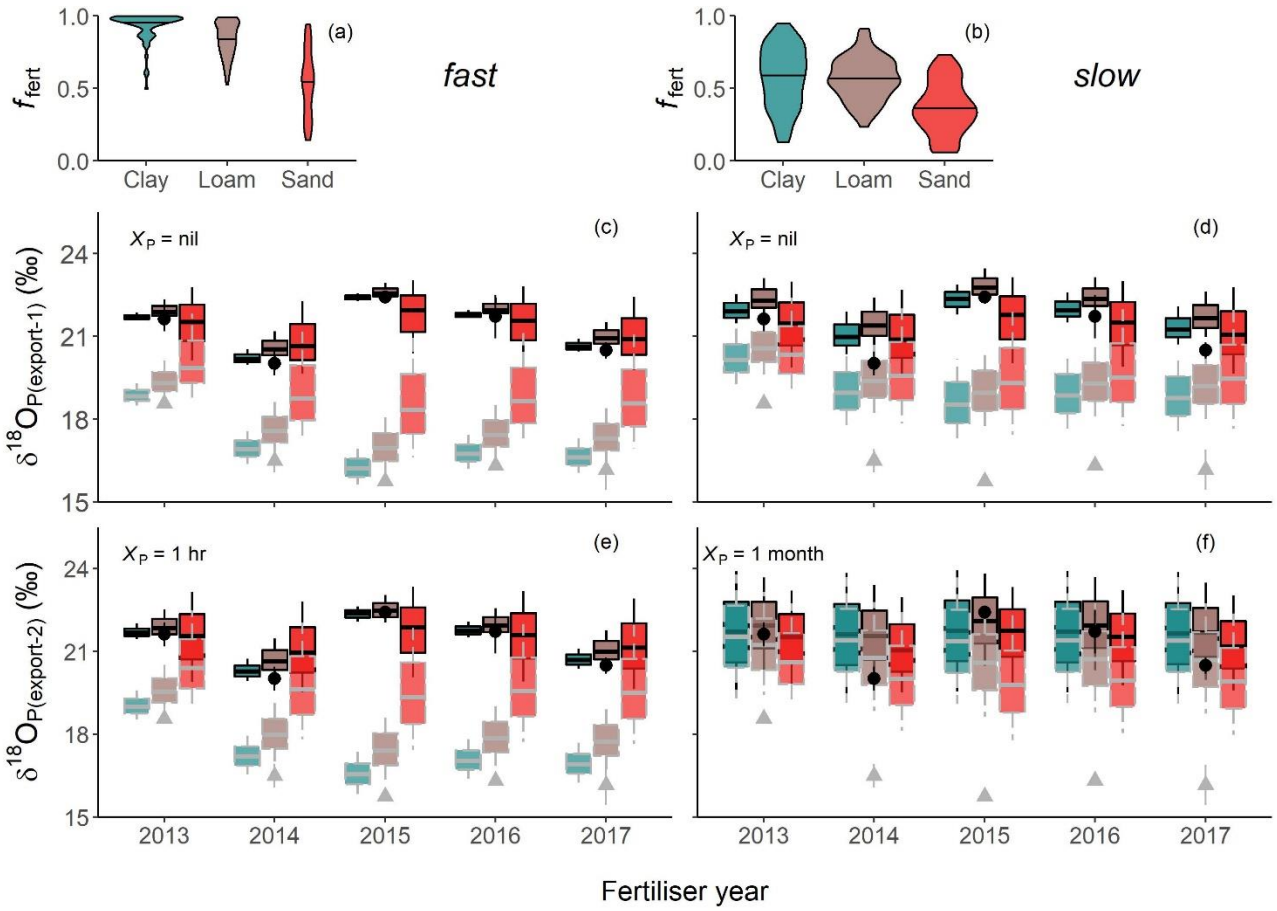

Fig. 4 The possible range of the isotopic composition of PO_4^{3-} export from clay, loam, and sand pasture soils ($\delta^{18}O_{P(export)}$, ‰ v. VSMOW) within a catchment depends on fertiliser contribution to the leachable soil PO_4^{3-} pool (f_{fert}) and fertiliser $\delta^{18}O_P$ composition (AG: black circles, SP: grey triangles, manufactured 2013-2017). $\delta^{18}O_{P(export)}$ values were calculated for two export scenarios: fast (a, c, e), where PO_4^{3-} is exported <1 day after fertilisation, and slow (b, d, f), where PO_4^{3-} is leached over weeks-months. Both fast and slow export could occur with (e, f: X_P = 1 h or 1 month) or without (c, d: X_P = nil) soil biological P turnover (Eq. 3). Violins (a, b) show the distribution of f_{fert} values around the mean (solid line); boxes (c-f) show the mean ± 1 SD for $\delta^{18}O_{P(export)}$, with whiskers to the minimum and maximum. Box colours distinguish soil textures (as defined in a and b) and outlines the fertiliser (AG: black, SP: grey).

4. Discussion

4.1 Fertilisers

The $\delta^{18}O_{P(fert)}$ range here (17 – 21 ‰) fits previous reports for inorganic commercial fertilisers (Table 2). Variations in $\delta^{18}O_{P(fert)}$ are generally attributed to geologic differences in the rocks sourced to make the fertilisers (Davies et al., 2014; Gruau et al., 2005). This is because the $\delta^{18}O_P$ composition of the sedimentary rocks sourced to produce PO_4^{3-} fertilisers depend on age and/or equilibration with $\delta^{18}O_{H2O}$ during formation (Sun et al., 2020). Here the ~8 ‰ difference between N-bearing (AG, MAP) and rock (SP) fertilisers corresponded with different geologic

source materials: AG and MAP were manufactured using materials from Florida, USA (Eocene – Miocene, ~55 MBP (Trueman, 1965)), while SP was manufactured using Christmas Island rocks (Oligocene – Pliocene, ~33 MBP (Van Kauwenbergh et al., 1990)). However, this explanation for the 5 - 8 ‰ difference between the fertiliser types does not hold up to scrutiny. The ~20 MY gap is negligible in geologic time (e.g., the 3 ‰ difference between PO_4^{3-} in China v the Middle East corresponds to ~300 MY (Sun et al., 2020)). Likewise, different $\delta^{18}O_{P(eq)}$ during formation is unlikely given similarities in the $\delta^{18}O_{H2O}$ and temperature regimens between the Indian Ocean and tropical Atlantic (LeGrande and Schmidt, 2006). This suggests that there is an additional factor than the commonly cited 'geologic $\delta^{18}O_P$ differences' that is contributing to the consistent offset between fertiliser types. We note that geology-driven variations in $\delta^{18}O_{P(fert)}$ is not robustly supported by the literature, with source material origins provided in only four of nine published studies (Table 2). This suggests that future work should encompass isotopic fractionation during manufacturing, which is theoretically possible given the filtration and solubilisation processes used (Chien et al., 2011), especially given the consistent differences between fertilisers made from raw (SP) v pre-processed (AG, MAP) materials. A similar mechanism was proposed to explain differences in tap water $\delta^{18}O_P$ (Gooddy et al., 2015), and requires further consideration.

Regardless of the exact driver (source, manufacturing), a single precise $\delta^{18}O_{P(fert)}$ value is unlikely to exist at the spatial and temporal scale of catchment studies. Establishing methods for predicting, and thus better constraining, $\delta^{18}O_{P(fert)}$ will be critical to any future attempts to use $\delta^{18}O_P$ to trace aquatic PO_4^{3-}. As first steps, we recommend future isotope studies report both the chemical form and geologic (rather than commercial) origin of P fertilisers.

4.2 Soils

Soil P variations fit expectations (Table 1, Fig. 2). P_{TIP} content was at the very low end for agricultural soils and C_{org}:P_{org} ratios at the high end for mineral soils, both typical for weathered southwestern Australian soils (Helfenstein et al., 2020; Spohn, 2020; Turner and Laliberte, 2015).

374 Phosphate partitioning followed the anticipated shift from sands with low, highly leachable, PO_4^{3-}
375 pools, to clays with larger, less leachable, PO_4^{3-} pools (Nash et al., 2019; O'Halloran et al., 1987).
376 These soil texture differences provide a solid basis to test how P buffering capacity controls
377 $\delta^{18}O_{P(soil)}$ and $\delta^{18}O_{P(export)}$.

378 $\delta^{18}O_{P(soil)}$ is hypothesised to reflect differences in the size and availability of soil PO_4^{3-}
379 (Bauke, 2020). Loosely bound PO_4^{3-} (H_2O or $NaHCO_3$ fractions) can be completely recycled in
380 days, whereas more tightly bound PO_4^{3-} (NaOH or HCl fractions) turnover may take centuries
381 (Helfenstein et al., 2020). Because biological PO_4^{3-} turnover moves $\delta^{18}O_{P(soil)}$ towards $\delta^{18}O_{P(eq)}$,
382 more labile PO_4^{3-} fractions tends to have (higher) $\delta^{18}O_P$ values closer to $\delta^{18}O_{P(eq)}$ and more tightly
383 bound PO_4^{3-} fractions tend to have (lower) $\delta^{18}O_{P(soil)}$ values closer to the geologic parent material
384 $\delta^{18}O_P$ (Roberts et al., 2015; Tian et al., 2020). This predicts that the sands' predominantly labile
385 PO_4^{3-} pool would shift $\delta^{18}O_{P(soil)}$ values higher than the clays, where most PO_4^{3-} is tightly bound
386 (Rodionov et al., 2020). Instead, the sands had the lowest $\delta^{18}O_{P(soil)}$ values, and almost all $\delta^{18}O_{P(soil)}$
387 values fell within the $\delta^{18}O_{P(eq)}$ range (Fig. 3). It is reasonable that all soil PO_4^{3-} was within the
388 $\delta^{18}O_{P(eq)}$ range as geologic PO_4^{3-} is unlikely to persist in any of these ~300,000 year old soils (Shen
389 et al., 2020; Turner and Laliberte, 2015). But if PO_4^{3-} is in isotopic equilibrium with soil water, why
390 do $\delta^{18}O_{P(soil)}$ values fall into distinct 'soil texture' zones within this range?

391 Variations within the $\delta^{18}O_{P(eq)}$ range could be driven by three factors: divergent equilibrium
392 conditions (soil temperature, $\delta^{18}O_{H2O}$), different PO_4^{3-} sources, and/or fractionation by competing
393 biological processes. First, daily – seasonal parameter fluctuations are not seen to affect $\delta^{18}O_{P(soil)}$ of
394 P_{TIP} (Angert et al., 2011; Lei et al., 2019). This suggests that long-term evaporation ($\delta^{18}O_{H2O}$) or
395 temperature differences between the soil textures would be needed to create a 'soil specific'
396 $\delta^{18}O_{P(eq)}$ range. Factors like slope, aspect, and vegetation (Hacker et al., 2019; Sprenger et al., 2016)
397 are excluded here due to the flat terrain and relatively homogenous land-use, but soil texture can
398 affect evaporation. However, a textural impact on evaporation would elevate $\delta^{18}O_{P(soil)}$ in coarse
399 grained sands above $\delta^{18}O_{P(soil)}$ in the fine grained clays (Gazis and Feng, 2004), the opposite of the

observed pattern. Second, pastures receive P_{org} and PO_4^{3-} inputs. Inorganic fertilisers can be ruled out as $\delta^{18}O_{P(fert)}$ values were lower than loam $\delta^{18}O_{P(soil)}$ (Fig. 4), and likewise processed P_{org} (manure) likely has $\delta^{18}O_P$ below the $\delta^{18}O_{P(soil)}$ range here (Granger et al., 2017b). While raw P_{org} inputs (plants) can have $\delta^{18}O_P$ up to ~30 ‰ (Pfahler et al., 2013; von Sperber et al., 2015), the mechanism through which they could differently affect soil textures under similar management (including pasture plants) is unclear. Charred organic matter is also a potentially significant P input (Baldock et al., 2013). A survey of nearby pastures suggests that loams contain more char than sands or clays (9.2 ± 2 mg C g^{-1} v 7.7 ± 2 mg C g^{-1} and 4.9 ± 2 mg C g^{-1}, respectively) (Viscarra Rossel et al., 2014). If char contains 20 µg PO_4^{3-}-P g^{-1} (Pluchon et al., 2015), this could be the source of 30% of loam PO_4^{3-}, v 5% of clay PO_4^{3-}. This is an intriguing possibility, but measurements of combusted organic material suggest char $\delta^{18}O_P$ values may be too low (~15 ‰) (Bigio and Angert, 2019) to explain the observed loam $\delta^{18}O_{P(soil)}$ values.

Alternatively, both the mineralisation of P_{org} to PO_4^{3-} and microbial PO_4^{3-} assimilation affect $\delta^{18}O_P$. Scavenging P_{org} in low fertility soils can decrease $\delta^{18}O_{P(soil)}$ below $\delta^{18}O_{P(eq)}$ (Liang and Blake, 2006; Pistocchi et al., 2020), and estimates suggest that mineralisation is highest (P_{min} = ~1% of P_{TIP} per fortnight) in the P-poor, relatively low $\delta^{18}O_{P(soil)}$ sands (Table 1). Additionally, microbial PO_4^{3-} assimilation increases $\delta^{18}O_{P(soil)}$ (Blake et al., 2005), with stronger fractionation when P is limiting (Lis et al., 2019). This gives a plausible explanation for the relatively high loam $\delta^{18}O_{P(soil)}$ values. Low P in both sands and loams could promote microbial PO_4^{3-} uptake and increase $\delta^{18}O_{P(soil)}$ of both soil textures (Bünemann et al., 2012), but the low sand C_{org} and P content causes its microbial P to be more efficiently recycled and $\delta^{18}O_{P(soil)}$ reset to the mean $\delta^{18}O_{P(eq)}$ range. This supports the assumption in catchment models that sand PO_4^{3-} is completely exhausted every winter (Summers et al., 1999). Although the exact driver of the soil textures $\delta^{18}O_{P(soil)}$ patterns is not certain, the non-random distribution of $\delta^{18}O_{P(soil)}$ within the $\delta^{18}O_{P(eq)}$ range emphasises the need to move beyond simply defining $\delta^{18}O_{P(soil)}$ as ‘in’ or ‘out’ of equilibrium and start unpicking the competing biological and hydrologic processes at play.

426

427 4.3 $\delta^{18}O_P$ as a tracer of PO_4^{3-} export from agricultural systems

428 There are three main questions about agricultural P export that $\delta^{18}O_P$ models look to answer:
429 1) how much fertiliser is exported directly to water?, 2) which landscape units contribute
430 disproportionately to PO_4^{3-} export?, and, 3) how much does agriculture contribute to catchment
431 PO_4^{3-} loads? The mixing models used here generated clear constraints on how $\delta^{18}O_P$ data could be
432 used at each of these scales.

433 Directly exported P fertilisers are a significant financial and environmental risk. Although
434 difficult to measure, estimates suggest fertilisers account for 30-80% of PO_4^{3-} leached from
435 agricultural systems (Nash et al., 2019), and radiotracer studies show 20-30 % of fertiliser PO_4^{3-} is
436 leached from pastures within two months of application (McLaren et al., 2017; McLaren et al.,
437 2016). There is further uncertainty about the timing of these direct export events: how long
438 fertilisers stay in granular form depends on rainfall, temperature, and fertiliser type (McLaren et al.,
439 2017). The wide $\delta^{18}O_{P(fert)}$ range reported here indicates that $\delta^{18}O_P$ values could prove a uniquely
440 powerful tool for untangling these PO_4^{3-} leaching dynamics at the plot - paddock scale if
441 isotopically distinct fertiliser v soils were first identified. Yet the same $\delta^{18}O_{P(fert)}$ range complicates
442 efforts to identify soil and land-use specific $\delta^{18}O_{P(export)}$ signatures (Fig. 4, Table 3).

443 The twin possibilities of mixed fertiliser use and variable biological P turnover drive the
444 uncertainty in $\delta^{18}O_{P(export)}$. Across the modelled two sub-catchments the 'agricultural' $\delta^{18}O_{P(export)}$
445 could reasonably range between 18‰ and 25‰, a much wider range than would be predicted by
446 simply using the sub-catchment soil maps to upscale $\delta^{18}O_{P(soil)}$. This level of uncertainty means
447 large datasets of receiving water $\delta^{18}O_P$ values are needed to generate statistically robust
448 identification of the fertiliser and soil PO_4^{3-} sources. For instance, measuring an 'out of equilibrium'
449 downstream $\delta^{18}O_P$ value of 19‰ could reasonably be evidence of SP export, but would not rule out
450 export of other fertilisers contributing up to 40% of PO_4^{3-}. Conversely, measuring a $\delta^{18}O_P$ value of
451 21‰, well above the SP $\delta^{18}O_{P(fert)}$ range, could not conclusively rule SP out as a PO_4^{3-} source (Fig.

4, Table 3). So while biological P turnover could ameliorate some of the variability created by fertiliser-soil mixing by shifting $\delta^{18}O_{P(export)}$ values towards $\delta^{18}O_{P(eq)}$, it also highlights more intransigent sources of uncertainty. First, the soil $\delta^{18}O_{P(eq)}$ range is itself uncertain due to questions around the extent to which variations are caused by hydrology (temperature and $\delta^{18}O_{H2O}$ (Benettin et al., 2018; Skrzypek et al., 2019)) v biology (balance between biological P cycling pathways (Helfenstein et al., 2018; Siegenthaler et al., 2020)). Second, evaluating these questions about soil $\delta^{18}O_{P(eq)}$ dynamics is complicated by the fact that the PO_4^{3-} pools that can be extracted for $\delta^{18}O_P$ analysis do not necessarily align with those that are environmentally relevant (Gu and Margenot, 2020; McConnell et al., 2020). Both situations contrast with the established approaches to tracing PO_4^{3-} pollution point sources like wastewater effluent (Gooddy et al., 2018), where biological modification of the defined source signature will occur post export to the waterway (Davies et al., 2014). The interconnected uncertainties about P turnover and $\delta^{18}O_{P(eq)}$ must be resolved in order to usefully incorporate $\delta^{18}O_P$ into P reactive transport models (Dorioz et al., 1998). One potential is that improved $\delta^{18}O_{P(eq)}$ understanding could be used to construct $\delta^{18}O_P$ catchment models based on temperature and $\delta^{18}O_{H2O}$ regimens.

5. Conclusions

The ability of phosphate isotopes ($\delta^{18}O_P$) to trace diffuse agricultural pollutants through catchments is limited by variations in soil zone inputs and reactions. The analytical template here highlights the importance, but also the limitations, of using site-specific $\delta^{18}O_{P(fert)}$ values to identify diffuse agricultural pollution. Uncertainty from $\delta^{18}O_P$ can reasonably be constrained via site-specific measurements in smaller catchments, but until biological turnover (fractionation and rates) is better defined surface water $\delta^{18}O_P$ signatures should be attributed to diffuse catchment sources with caution.

Associated content: The Supporting Information pdf contains additional: S1) site maps (Figure S1: Site map with farm locations, Figure S2: Sub-catchment maps with soil textures), S2) additional soil data (Table S1: Background data on soil P status and N content, Table S2: Sequential extraction soil PO_4^{3-} concentration information by farm × soil texture, Table S3: $P_{min(14)}$ data), S3) input variables for $\delta^{18}O_{P(eq)}$ and mixing model calculations (Table S4: precipitation $\delta^{18}O_{H2O}$ for winter 2017, Table S5: Long-term soil temperature data, Table S6: Modelled daily winter soil temperatures, Table S7: Estimated P turnover (X_P) by soil texture), and, S4) R scripts (S4.1: $\delta^{18}O_{P(eq)}$ calculations,S4.2: mixing models, S4.3: up-scaling calculations). Soil data are available on https://figshare.com/s/e1416e6217fe0e7f3b10 (*link for review only, will be published with DOI upon acceptance*).

Acknowledgements: Iain Alexander and Natasha Carlson-Perret (Southern Cross University) assisted with soil P extractions. Robert Summers (Department of Primary Industries and Regional Development, Western Australia) supplied background site data, soil sampling equipment, and fertiliser samples. Fiona Valesini (Murdoch University) helped organise field work and secure research funding. Thanks to Justin Mercy (CSBP) for information on fertiliser sources and production, and to the six land owners for granting access to their properties. Research was funded by Australian Research Council grant LP150100451 and by the UK's Natural Environment Research Council Environmental Isotope Facility grant IP-1664-1116.

Author contributions: NSW, MYR, and BDE designed the study. NSW and MYR carried out the study. PJW and ACS carried out isotopic extractions and analysed the samples. NSW and DCG analysed the data. NSW and DCG wrote the manuscript, with input from all co-authors.

References

Achat, D.L., Bakker, M.R., Zeller, B., Pellerin, S., Bienaimé, S., Morel, C., 2010. Long-term organic phosphorus mineralization in Spodosols under forests and its relation to carbon and nitrogen mineralization. Soil Biol. Biochem. 42, 1479-1490.

Angert, A., Weiner, T., Mazeh, S., Tamburini, F., Frossard, E., Bernasconi, S.M., Sternberg, M., 2011. Seasonal variability of soil phosphate stable oxygen isotopes in rainfall manipulation experiments. Geochim. Cosmochim. Acta 75, 4216-4227.

Baldock, J.A., Sanderman, J., Macdonald, L.M., Puccini, A., Hawke, B., Szarvas, S., McGowan, J., 2013. Quantifying the allocation of soil organic carbon to biologically significant fractions. Soil Res. 51, 561-576.

Bauke, S.L., 2020. Game changer in soil science: Perspectives from the Fritz-Scheffer awardee. Oxygen isotopes in phosphate-The key to phosphorus tracing? J. Plant Nutr. Soil Sci., 8.

Benettin, P., Volkmann, T.H.M., von Freyberg, J., Frentress, J., Penna, D., Dawson, T.E., Kirchner, J., 2018. Effects of climatic seasonality on the isotopic composition of evaporating soil waters. Hydrol. Earth Syst. Sci. 22, 2881-2890.

Beusen, A.H.W., Bouwman, A.F., Van Beek, L.P.H., Mogollon, J.M., Middelburg, J.J., 2016. Global riverine N and P transport to ocean increased during the 20th century despite increased retention along the aquatic continuum. Biogeosci. 13, 2441-2451.

Bigio, L., Angert, A., 2019. Oxygen isotope signatures of phosphate in wildfire ash. ACS Earth Space Chem. 3, 760-769.

Blake, R.E., O'Neil, J.R., Surkov, A.V., 2005. Biogeochemical cycling of phosphorus: Insights from oxygen isotope effects of phosphoenzymes. American Journal of Science 305, 596-620.

Bolland, M.D.A., Allen, D.G., 1998. Spatial variation of soil test phosphorus and potassium, oxalate-extractable iron and aluminum, phosphorus-retention index, and organic carbon content in soils of Western Australia. Commun. Soil Sci. Plant Anal. 29, 381-392.

Bünemann, E.K., Oberson, A., Liebisch, F., Keller, F., Annaheim, K.E., Huguenin-Elie, O., Frossard, E., 2012. Rapid microbial phosphorus immobilization dominates gross phosphorus fluxes in a grassland soil with low inorganic phosphorus availability. Soil Biol. Biochem. 51, 84-95.

Chang, S.J., Blake, R.E., 2015. Precise calibration of equilibrium oxygen isotope fractionations between dissolved phosphate and water from 3 to 37 degrees C. Geochim. Cosmochim. Acta 150, 314-329.

Chien, S.H., Prochnow, L.I., Tu, S., Snyder, C.S., 2011. Agronomic and environmental aspects of phosphate fertilizers varying in source and solubility: an update review. Nutr. Cycl. Agroecosys. 89, 229-255.

Davies, C.L., Surridge, B.W.J., Gooddy, D.C., 2014. Phosphate oxygen isotopes within aquatic ecosystems: Global data synthesis and future research priorities. Sci. Total Environ. 496, 563-575.

Dorioz, J.M., Cassell, E.A., Orand, A., Eisenman, K.G., 1998. Phosphorus storage, transport and export dynamics in the Foron River watershed. Hydrol. Process. 12, 285-309.

Gazis, C., Feng, X.H., 2004. A stable isotope study of soil water: evidence for mixing and preferential flow paths. Geoderma 119, 97-111.

Gooddy, D.C., Bowes, M.J., Lapworth, D.J., Lamb, A.L., Williams, P.J., Newton, R.J., Davies, C.L., Surridge, B.W.J., 2018. Evaluating the stable isotopic composition of phosphate oxygen as a tracer of phosphorus from waste water treatment works. Appl. Geochem. 95, 139-146.

Gooddy, D.C., Lapworth, D.J., Ascott, M.J., Bennett, S.A., Heaton, T.H.E., Surridge, B.W.J., 2015. Isotopic fingerprint for phosphorus in drinking water supplies. Environ. Sci. Technol. 49, 9020-9028.

Gooddy, D.C., Lapworth, D.J., Bennett, S.A., Heaton, T.H.E., Williams, P.J., Surridge, B.W.J., 2016. A multi-stable isotope framework to understand eutrophication in aquatic ecosystems. Water Res. 88, 623-633.

552 Granger, S.J., Harris, P., Peukert, S., Guo, R., Tamburini, F., Blackwell, M.S.A., Howden, N.J.K.,
553 McGrath, S., 2017a. Phosphate stable oxygen isotope variability within a temperate agricultural
554 soil. Geoderma 285, 64-75.
555 Granger, S.J., Heaton, T.H.E., Pfahler, V., Blackwell, M.S.A., Yuan, H.M., Collins, A.L., 2017b.
556 The oxygen isotopic composition of phosphate in river water and its potential sources in the Upper
557 River Taw catchment, UK. Sci. Total Environ. 574, 680-690.
558 Gross, A., Angert, A., 2015. What processes control the oxygen isotopes of soil bio-available
559 phosphate? Geochim. Cosmochim. Acta 159, 100-111.
560 Gruau, G., Legeas, M., Riou, C., Gallacier, E., ois Martineau, F., Henin, O., 2005. The oxygen
561 isotope composition of dissolved anthropogenic phosphates: a new tool for eutrophication research?
562 Water Res. 39, 232-238.
563 Gu, C., Margenot, A.J., 2020. Navigating limitations and opportunities of soil phosphorus
564 fractionation. Plant Soil.
565 Hacker, N., Wilcke, W., Oelmann, Y., 2019. The oxygen isotope composition of bioavailable
566 phosphate in soil reflects the oxygen isotope composition in soil water driven by plant diversity
567 effects on evaporation. Geochim. Cosmochim. Acta 248, 387-399.
568 Haygarth, P.M., Condron, L.M., Heathwaite, A.L., Turner, B.L., Harris, G.P., 2005. The
569 phosphorus transfer continuum: Linking source to impact with an interdisciplinary and multi-scaled
570 approach. Sci. Total Environ. 344, 5-14.
571 Hedley, M.J., Stewart, J.W.B., Chauhan, B.S., 1982. Changes in inorganic and organic soil
572 phosphorus fractions induced by cultivation practices and by laboratory incubations. Soil Sci. Soc.
573 Am. J. 46, 970-976.
574 Helfenstein, J., Pistocchi, C., Oberson, A., Tamburini, F., Goll, D.S., Frossard, E., 2020. Estimates
575 of mean residence times of phosphorus in commonly considered inorganic soil phosphorus pools.
576 Biogeosci. 17, 441-454.
577 Helfenstein, J., Tamburini, F., von Sperber, C., Massey, M.S., Pistocchi, C., Chadwick, O.A.,
578 Vitousek, P.M., Kretzschmar, R., Frossard, E., 2018. Combining spectroscopic and isotopic
579 techniques gives a dynamic view of phosphorus cycling in soil. Nat. Commun. 9, 9.
580 Henry, L., Wickham, H., 2020. purrr: Functional Programming Tools, R package version 0.3.4.,
581 https://CRAN.R-project.org/package=purrr.
582 Hollins, S.E., Hughes, C.E., Crawford, J., Cendón, D.I., Meredith, K.T., 2018. Rainfall isotope
583 variations over the Australian continent – Implications for hydrology and isoscape applications. Sci.
584 Total Environ. 645, 630-645.
585 IAEA/WMO, 2020. Global Network of Isotopes in Precipitation.
586 Ishida, T., Uehara, Y., Iwata, T., Cid-Andres, A.P., Asano, S., Ikeya, T., Osaka, K., Ide, J.,
587 Privaldos, O.L.A., De Jesus, I.B.B., Peralta, E.M., Trino, E.M.C., Ko, C.Y., Paytan, A., Tayasu, I.,
588 Okuda, N., 2019. Identification of phosphorus sources in a watershed using a phosphate oxygen
589 isoscape approach. Environ. Sci. Technol. 53, 4707-4716.
590 Jaisi, D.P., Kukkadapu, R.K., Stout, L.M., Varga, T., Blake, R.E., 2011. Biotic and abiotic
591 pathways of phosphorus cycling in minerals and sediments: Insights from oxygen isotope ratios in
592 phosphate. Environ. Sci. Technol. 45, 6254-6261.
593 Jensen, J.L., Christensen, B.T., Schjønning, P., Watts, C.W., Munkholm, L.J., 2018. Converting
594 loss-on-ignition to organic carbon content in arable topsoil: pitfalls and proposed procedure. Eur. J.
595 Soil Sci. 69, 604-612.
596 Kassambara, A., 2020. rstatix: Pipe-Friendly Framework for Basic Statistical Tests, R package
597 version 0.5.0 ed, https://CRAN.R-project.org/package=rstatix.
598 Kearney, M.R., 2019. MicroclimOz – A microclimate data set for Australia, with example
599 applications. Austral Ecol. 44, 534-544.
600 LeGrande, A.N., Schmidt, G.A., 2006. Global gridded data set of the oxygen isotopic composition
601 in seawater. Geophys. Res. Lett. 33, 5.

Lei, X.T., Chen, M., Guo, L.D., Zhang, X.G., Jiang, Z.H., Chen, Z.G., 2019. Diurnal variations in the content and oxygen isotope composition of phosphate pools in a subtropical agriculture soil. Geoderma 337, 863-870.
Li, X., Wang, Y., Stern, J., Cu, B.H., 2011. Isotopic evidence for the source and fate of phosphorus in Everglades wetland ecosystems. Appl. Geochem. 26, 688-695.
Liang, Y., Blake, R.E., 2006. Oxygen isotope signature of P-i regeneration from organic compounds by phosphomonoesterases and photooxidation. Geochim. Cosmochim. Acta 70, 3957-3969.
Lis, H., Weiner, T., Pitt, F.D., Keren, N., Angert, A., 2019. Phosphate uptake by cyanobacteria is associated with kinetic fractionation of phosphate oxygen isotopes. ACS Earth Space Chem. 3, 233-239.
McArthur, W.M., Bettenay, E., 1974. The development and distribution of the soils of the Swan Coastal Plain, Western Australia, 2nd ed. CSIRO, Melbourne, Australia.
McConnell, C.A., Kaye, J.P., Kemanian, A.R., 2020. Reviews and syntheses: Ironing out wrinkles in the soil phosphorus cycling paradigm. Biogeosci. 17, 5309-5333.
McLaren, T.I., McBeath, T.M., Simpson, R.J., Richardson, A.E., Stefanski, A., Guppy, C.N., Smernik, R.J., Rivers, C., Johnston, C., McLaughlin, M.J., 2017. Direct recovery of P-33-labelled fertiliser phosphorus in subterranean clover (Trifolium subterraneum) pastures under field conditions - The role of agronomic management. Agric. Ecosyst. Environ. 246, 144-156.
McLaren, T.I., McLaughlin, M.J., McBeath, T.M., Simpson, R.J., Smernik, R.J., Guppy, C.N., Richardson, A.E., 2016. The fate of fertiliser P in soil under pasture and uptake by subterraneum clover - a field study using P-33-labelled single superphosphate. Plant Soil 401, 23-38.
McLaughlin, K., Cade-Menun, B.J., Paytan, A., 2006. The oxygen isotopic composition of phosphate in Elkhorn Slough, California: A tracer for phosphate sources. Estuar. Coast. Shelf Sci. 70, 499-506.
Melland, A.R., Fenton, O., Jordan, P., 2018. Effects of agricultural land management changes on surface water quality: A review of meso-scale catchment research. Environ. Sci. Policy 84, 19-25.
Metson, G.S., Lin, J.J., Harrison, J.A., Compton, J.E., 2017. Linking terrestrial phosphorus inputs to riverine export across the United States. Water Res. 124, 177-191.
Nash, D.M., McDowell, R.W., Condron, L.M., McLaughlin, M.J., 2019. Direct exports of phosphorus from fertilizers applied to grazed pastures. J. Environ. Qual. 48, 1380-1396.
O'Halloran, I.P., Stewart, J.W.B., Kachanoski, R.G., 1987. Influence of texture and management practices on the forms and distribution of soil phosphorus. Can. J. Soil Sci. 67, 147-163.
Paytan, A., Roberts, K., Watson, S., Peek, S., Chuang, P.C., Defforey, D., Kendall, C., 2017. Internal loading of phosphate in Lake Erie Central Basin. Sci. Total Environ. 579, 1356-1365.
Pedersen, T.L., 2019. patchwork: The Composer of Plots, R package version 1.0.0 ed, https://CRAN.R-project.org/package=patchwork.
Pfahler, V., Durr-Auster, T., Tamburini, F., Bernasconi, S., Frossard, E., 2013. 18O enrichment in phosphorus pools extracted from soybean leaves. New Phytol. 197, 186-193.
Pistocchi, C., Meszaros, E., Frossard, E., Bunemann, E.K., Tamburini, F., 2020. In or out of equilibrium? How microbial activity controls the oxygen isotopic composition of phosphate in forest organic horizons with low and high phosphorus availability. Front. Environ. Sci. 8, 15.
Pistocchi, C., Tamburini, F., Gruau, G., Ferhi, A., Trevisan, D., Dorioz, J.M., 2017. Tracing the sources and cycling of phosphorus in river sediments using oxygen isotopes: Methodological adaptations and first results from a case study in France. Water Res. 111, 346-356.
Pluchon, N., Casetou, S.C., Kardol, P., Gundale, M.J., Nilsson, M.C., Wardle, D.A., 2015. Influence of species identity and charring conditions on fire-derived charcoal traits. Can. J. For. Res. 45, 1669-1675.
Polain, K., Guppy, C., Knox, O., Lisle, L., Wilson, B., Osanai, Y., Siebers, N., 2018. Determination of agricultural impact on soil microbial activity using delta O-18(p) (HCI) and respiration experiments. ACS Earth Space Chem. 2, 683-691.

Rivers, M.R., Weaver, D.M., Smettem, K.R.J., Davies, P.M., 2013. Estimating farm to catchment nutrient fluxes using dynamic simulation modelling – Can agri-environmental BMPs really do the job? J Environ Manage 130, 313-323.
Roberts, K., Defforey, D., Turner, B.L., Condron, L.M., Peek, S., Silva, S., Kendall, C., Paytan, A., 2015. Oxygen isotopes of phosphate and soil phosphorus cycling across a 6500 year chronosequence under lowland temperate rainforest. Geoderma 257–258, 14-21.
Rodionov, A., Bauke, S.L., von Sperber, C., Hoeschen, C., Kandeler, E., Kruse, J., Lewandowski, H., Marhan, S., Mueller, C.W., Simon, M., Tamburini, F., Uhlig, D., von Blanckenburg, F., Lang, F.D., Amelung, W., 2020. Biogeochemical cycling of phosphorus in subsoils of temperate forest ecosystems. Biogeochem. 150, 313-328.
Rupp, H., Meissner, R., Leinweber, P., 2018. Plant available phosphorus in soil as predictor for the leaching potential: Insights from long-term lysimeter studies. Ambio 47, 103-113.
Saunders, W.M.H., Williams, E.G., 1955. Observations on the determination of total organic phosphorus in soils. J. Soil Sci. 6, 254-267.
Shen, J., Smith, A.C., Claire, M.W., Zerkle, A.L., 2020. Unraveling biogeochemical phosphorus dynamics in hyperarid Mars-analogue soils using stable oxygen isotopes in phosphate. Geobiology 18, 760-779.
Siegenthaler, M.B., Tamburini, F., Frossard, E., Chadwick, O., Vitousek, P., Pistocchi, C., Meszaros, V., Helfenstein, J., 2020. A dual isotopic (P-32 and O-18) incubation study to disentangle mechanisms controlling phosphorus cycling in soils from a climatic gradient (Kohala, Hawaii). Soil Biol. Biochem. 149, 12.
Skrzypek, G., Dogramaci, S., Page, G.F.M., Rouillard, A., Grierson, P.F., 2019. Unique stable isotope signatures of large cyclonic events as a tracer of soil moisture dynamics in the semiarid subtropics. J. Hydrol. 578, 13.
Spohn, M., 2020. Increasing the organic carbon stocks in mineral soils sequesters large amounts of phosphorus. Global Change Biol. 26, 4169-4177.
Sprenger, M., Leistert, H., Gimbel, K., Weiler, M., 2016. Illuminating hydrological processes at the soil-vegetation-atmosphere interface with water stable isotopes. Rev. Geophys. 54, 674-704.
Sprenger, M., Tetzlaff, D., Soulsby, C., 2017. Soil water stable isotopes reveal evaporation dynamics at the soil-plant-atmosphere interface of the critical zone. Hydrol. Earth Syst. Sci. 21, 3839-3858.
Summers, R.N., Van Gool, D., Guise, N.R., Heady, G.J., Allen, T., 1999. The phosphorus content in the run-off from the coastal catchment of the Peel Inlet and Harvey Estuary and its associations with land characteristics. Agric. Ecosyst. Environ. 73, 271-279.
Summers, R.N., Weaver, D.M., 2011. Soil test and phosphorus rate for high rainfall clover pastures. Bulletin 4829.
Sun, Y., Amelung, W., Wu, B., Haneklaus, S., Maekawa, M., Lucke, A., Schnug, E., Bol, R., 2020. 'Co-evolution' of uranium concentration and oxygen stable isotope in phosphate rocks. Appl. Geochem. 114, 9.
Tamburini, F., Bernasconi, S.M., Angert, A., Weiner, T., Frossard, E., 2010. A method for the analysis of the $\delta^{18}O$ of inorganic phosphate extracted from soils with HCl. Eur. J. Soil Sci. 61, 1025-1032.
Tian, L.Y., Guo, Q.J., Yu, G.R., Zhu, Y.G., Lang, Y.C., Wei, R.F., Hu, J., Yang, X.R., Ge, T.D., 2020. Phosphorus fractions and oxygen isotope composition of inorganic phosphate in typical agricultural soils. Chemosphere 239, 10.
Tonderski, K., Andersson, L., Lindstrom, G., St Cyr, R., Schonberg, R., Taubald, H., 2017. Assessing the use of delta O-18 in phosphate as a tracer for catchment phosphorus sources. Sci. Total Environ. 607, 1-10.
Trueman, N.A., 1965. The phosphate, volcanic and carbonate rocks of Christmas Island (Indian Ocean). Journal of the Geological Society of Australia 12, 261-283.

703 Turner, B.L., Laliberte, E., 2015. Soil development and nutrient availability along a 2 million-year
704 coastal dune chronosequence under species-rich Mediterranean shrubland in southwestern
705 Australia. Ecosystems 18, 287-309.
706 Valesini, F.J., Hallett, C.S., Hipsey, M.R., Kilminster, K.L., Huang, P., Hennig, K., 2019. Chapter 7
707 - Peel-Harvey Estuary, Western Australia, in: Wolanski, E., Day, J.W., Elliott, M., Ramachandran,
708 R. (Eds.), Coasts and Estuaries. Elsevier, pp. 103-120.
709 Van Kauwenbergh, S.J., Cathcart, J.B., McClellan, G.H., 1990. Mineralogy and alteration of the
710 phosphate deposits of Florida : a detailed study of the mineralogy and chemistry of the phosphate
711 deposits of Florida, United States Geological Survey Bulletin.
712 Viscarra Rossel, R.A., Webster, R., Bui, E.N., Baldock, J., 2014. Baseline map of Australian soil
713 organic carbon stocks and their uncertainty., in: CSIRO (Ed.), Data Collection, v2 ed.
714 von Sperber, C., Tamburini, F., Brunner, B., Bernasconi, S.M., Frossard, E., 2015. The oxygen
715 isotope composition of phosphate released from phytic acid by the activity of wheat and Aspergillus
716 niger phytase. Biogeosci. 12, 4175-4184.
717 Wan, H., Liu, W.G., 2016. An isotope study (delta O-18 and delta D) of water movements on the
718 Loess Plateau of China in arid and semiarid climates. Ecol. Eng. 93, 226-233.
719 Wang, Y., Bauke, S.L., von Sperber, C., Tamburini, F., Guigue, J., Winkler, P., Kaiser, K.,
720 Honermeier, B., Amelung, W., 2021. Soil phosphorus cycling is modified by carbon and nitrogen
721 fertilization in a long-term field experiment. J. Plant Nutr. Soil Sci. 184, 282-293.
722 Weller, H., 2019. countcolors: Locates and Counts Pixels Within Color Range(s) in Images, R
723 package version 0.9.1.
724 Wickham, C., 2018. munsell: Utilities for Using Munsell Colours, R package version 0.5.0,
725 https://CRAN.R-project.org/package=munsell.
726 Wickham, H., 2016. ggplot2: Elegant Graphics for Data Analysis. Springer-Verlag New York,
727 https://ggplot2.tidyverse.org.
728 Young, M.B., McLaughlin, K., Kendall, C., Stringfellow, W., Rollog, M., Elsbury, K., Donald, E.,
729 Paytan, A., 2009. Characterizing the oxygen isotopic composition of phosphate sources to aquatic
730 ecosystems. Environ. Sci. Technol. 43, 5190-5196.
731

Tables

Table 1: Characteristics of pasture soils (0 – 10 cm) with contrasting textures (sand, clay, loam) collected from six farms (F1 – F6) across the coastal Peel-Harvey catchment in southwestern Western Australia (see SI S1 maps). Sample numbers indicate the total bulked (n = 3) cores collected for P content and the subset analysed for $\delta^{18}O_{P(soil)}$. The contribution of P_{org} to P_{total} is calculated on a g/g basis. Potential P mineralisation over 14 days ($P_{min(14)}$) is reported relative to the total HCl extractable PO_4^{3-} concentration (P_{TIP}). See SI S2 for additional soil chemistry data.

Texture	**Farm**	**sample #s**		**pH**	**C_{org}**	**P_{total}**	**% P_{org}**	**C_{org}:P_{org}**	$P_{min(14)}$:P_{TIP}
		all	*$\delta^{18}O_P$*		*mg C g^{-1}*	*µg P g^{-1}*	*(P_{org}/P_{total}) ·100*	g/g	mg/g
Clay	F3	3	1	5.8 (0.1)	33	390 (70)	33 (9)	290 (100)	0.27 (0.07)
	F4	9	4	6.5 (0.3)	68 (20)	450 (200)	37 (7)	440 (100)	0.68 (0.3)
	F6	9	3	6.3 (0.1)	76 (20)	250 (60)	46 (7)	700 (300)	0.90 (0.4)
Loam	F2	6	4	6.1 (0.09)	34 (9)	150 (50)	41 (7)	590 (200)	6.6 (4)
	F4	3	2	6.4 (0.06)	58 (20)	320 (100)	37 (10)	540 (200)	1.9 (2)
	F5	9	3	6.3 (0.2)	38 (10)	170 (50)	51 (8)	490 (200)	3.9 (2)
Sand	F1	9	4	5.8 (0.3)	46 (40)	470 (600)	53 (10)	340 (200)	7.7 (7)
	F2	6	2	6.3 (0.09)	54 (30)	120 (80)	55 (10)	1000 (600)	18 (10)
	F3	9	2	6.2 (0.1)	16 (7)	63 (20)	61 (20)	510 (200)	16 (10)

739 **Table 2** Inorganic fertiliser $\delta^{18}O_P$ values reported for this study and others ($\delta^{18}O_{P(fert)}$, values in ‰ v VSMOW), with respect to fertiliser type, where
740 the fertiliser was manufactured, and where the PO_4^{3-} raw material was sourced from ('unspecified' denotes data unavailable).
741

Fertiliser type	Manufactured	Sourced	$\delta^{18}O_{P(fert)}$	Reference
Superphosphate	Australia	Christmas Island	16.7 ± 1 *15.6 – 18.7*	This study
	Europe	*Unspecified*	17.7 ± 0.2	Tamburini et al. (2010)
	Japan	Japan	12.7	Ishida et al. (2019)
	Australia	*Unspecified*	21.4 ± 0.5	Polain et al. (2018)
	Israel	*Unspecified*	21.8 ± 0.3	(Gross and Angert, 2015)
	Europe	Morocco & USA	23 ± 0.3	Gruau et al. (2005)
Monoammonium phosphate	Australia	USA	21.6 ± 0.05	This study
	Australia	*Unspecified*	20.2 ± 0.1	Polain et al. (2018)
N-P-S-K	Australia	USA	21.3 ± 1 *19.7 – 22.4*	This study
	Europe	Morocco & USA	21.8 ± 0.5	Gruau et al. (2005)
	Europe	*Unspecified*	20.9 ± 6	Granger et al. (2017b)
Unspecified	USA	USA	23.8 ± 1	Li et al. (2011)
	USA	*Unspecified*	19 ± 1	McLaughlin et al. (2006)
	USA	Israel	19.6	Young et al. (2009)
	China	China	11.5 ± 0.1	Tian et al. (2020)

742

743
744

Table 3 Possible $\delta^{18}O_{P(export)}$ range from two sub-catchments with differing soil distributions (maps: SI S1). The $\delta^{18}O_{P(export)}$ range was calculated by varying the relative proportion of SP v AG fertilisers and speed of PO_4^{3-} transport from soil to water (fast, scenario a: mixing with H_2O extractable PO_4^{3-} pool, X_P = 0%; or scenario d: mixing with H_2O+$NaHCO_3$ extractable PO_4^{3-}, X_P = 20 – 90%, depending on soil texture), see SI S4 for calculations.

Sub-catchment	*Fertiliser*	**$\delta^{18}O_{P(export)}$ range** *Transport*	
		Fast+Slow[1] →	Mostly slow[2]
Pinjarra *19% clay, 4.4% loam, 76% sand*	1 SP + 0 AG	17.7 – 21.3	18.5 – 20.5
	0.6 SP + 0.4 AG	18.7 – 21.9	19.1 – 22.6
Harvey *21% clay, 29% loam, 50% sand*	1 SP + 0 AG	17.7 – 21.1	18.7 – 20.5
	0.6 SP + 0.4 AG	18.8 – 23.0	19.2 – 24.9

[1] 50% ‘d’ + 50% ‘a’

[2] 90% ‘d’ + 10% ‘a’

768 **Figure captions**

769 **Fig. 1** Two-pool isotope mixing models (Eq. 2, Eq. 3) constrained the possible $\delta^{18}O_P$ range of PO_4^{3-}
770 exported (leaching, run-off) from fertilised soils ($\delta^{18}O_{P(export)}$). The model was solved using
771 recommended low, moderate, and high fertiliser applications rate (P_{fert}, in µg P g^{-1} soil) for each soil
772 texture (clay, loam, sand) and $\delta^{18}O_{P(fert)}$ values for two fertilisers (AG: N-P-K, SP: superphosphate)
773 manufactured between 2013 and 2017. $\delta^{18}O_{P(fert)}$ for each year × fertiliser were 'mixed' with each
774 soil texture using the measured $\delta^{18}O_{P(soil)}$ range for P_{TIP} and P_{soil} (µg P g^{-1} soil), defined by H_2O
775 extractable PO_4^{3-} for fast export scenarios (a, c) and H_2O + $NaHCO_3$ extractable PO_4^{3-} for
776 slow/seasonal export scenarios (b, c). $\delta^{18}O_{P(export)}$ for both fast and slow export was calculated with
777 (c, d) and without (a, b) soil biological P turnover (X_P), which shifts $\delta^{18}O_{P(export)}$ towards $d^{18}O_{P(eq)}$
778 (Eq. 1). Fast export X_P (c) was approximated by $[P_{H2O} \cdot e\text{^}(\log(100+P_{H2O})/100 \cdot 1)]/P_{TIP}$ and slow
779 export X_P (d) by $[P_{NaOH} \cdot e\text{^}(\log(100+P_{NaOH})/100 \cdot 1)]/P_{TIP}$. Arrows indicate the same values were
780 applied across all soil textures, otherwise soil-specific values (mean±SD) were used. See SI S4 for
781 model scripts.

782

783 **Fig. 2** Phosphate in surface soils (0 – 10 cm) of 21 pastures with different textures in the Peel-
784 Harvey catchment (Western Australia) based on sequential extraction with H_2O (left, light outline),
785 $NaHCO_3$, NaOH, and HCl (right, dark outline). P_{TIP} concentrations (sum of four fractions) for each
786 soil texture is indicated at the top, and the percentage contribution of H_2O (easily leachable) and
787 H_2O+$NaHCO_3$ (seasonally leachable) fractions indicated with dashed lines. Boxes represent median
788 ± 1 SD.

789

790 **Fig. 3** The $\delta^{18}O_P$ of P_{TIP} in pasture soils (0-10 cm) classed as either clay, loam, or sand from six
791 farms across the Peel-Harvey catchment (Western Australia). Boxes represent median ± 1 SD for
792 each soil texture. Black lines represent the mean (solid line), ±1 SD (dashed lines), and

793 minimum/maximum (dotted lines) of the long-term local $\delta^{18}O_{P(eq)}$ range (Eq. 2); the grey line
794 indicates the mean $\delta^{18}O_{P(eq)}$ calculated for conditions during the winter sampling (*eq*-*w*).
795
796 **Fig. 4** The possible range of the isotopic composition of PO_4^{3-} export from clay, loam, and sand
797 pasture soils ($\delta^{18}O_{P(export)}$, ‰ v. VSMOW) within a catchment depends on fertiliser contribution to
798 the leachable soil PO_4^{3-} pool (f_{fert}) and fertiliser $\delta^{18}O_P$ composition (AG: black circles, SP: grey
799 triangles, manufactured 2013-2017). $\delta^{18}O_{P(export)}$ values were calculated for two export scenarios:
800 fast (a, c, e), where PO_4^{3-} is exported <1 day after fertilisation, and slow (b, d, f), where PO_4^{3-} is
801 leached over weeks-months. Both fast and slow export could occur with (e, f: X_P = 1 h or 1 month)
802 or without (c, d: X_P = nil) soil biological P turnover (Eq. 3). Violins (a, b) show the distribution of
803 f_{fert} values around the mean (solid line); boxes (c-f) show the mean ± 1 SD for $\delta^{18}O_{P(export)}$, with
804 whiskers to the minimum and maximum. Box colours distinguish soil textures (as defined in a and
805 b) and outlines the fertiliser (AG: black, SP: grey).
806